Electronic Supplementary Information

Excitation and analyzation of different surface plasmon modes on a suspended Ag nanowire

Yunkun Wu,[1,2] Liu Lu,[3] Lantian Feng,[1,2] Yang Chen,[1,2] XiaoZhuo Qi,[1,2] Hong-Liang Ren,[4] Guang-Can Guo,[1,2] and Xifeng Ren,[1,2,*]

[1]*Key Lab of Quantum Information, University of Science and Technology of China, CAS, Hefei, Anhui, 230026, China.*

[2]*Synergetic Innovation Center of Quantum Information & Quantum Physics, University of Science and Technology of China, Hefei, Anhui 230026, China*

[3]*School of Mechanical Engineering, Jiangsu University, Zhenjiang 212013, China*

[4]*College of Information Engineering, Zhejiang University of Technology, Hangzhou 310023, P.R. China*

**Address correspondence to: renxf@ustc.edu.cn*

Ⅰ. SAMPLE PREPARATION

In our experiment, fiber tapers were fabricated by stretching a single-mode fiber from opposite ends while heating it. The stretching force determined the cone angle of the fiber taper. Silver nanowires were synthesized via a chemical method, in which silver nitrate ($AgNO_3$) was chemically reacted with ethylene glycol in the presence of polyvinyl pyrrolidone (PVP). Then the solution was dripped onto an edge area of a side-polished substrate after the silver nanowires were purified from the reaction product and diluted. One nanowire was moved to the edge with a fiber taper until half of it was standing freely in air. Another fiber taper was moved close to the nanowire with a three-dimensional stage. The silver nanowire would stably adhere to the surface of the fiber taper for several hours by virtue of the van der Waals forces between them. Attaching the nanowire to the fiber taper with glue could further improve the stability. The ratio of the power after the confocal system to the power of the light sent to the single-mode fiber was approximately 20.6% (when the incident radiation was H polarized). An even higher efficiency could be achieved by modulating the coupling length and the taper angle of the fiber taper. Figure S1 shows a schematic diagram of the fabrication procedure of the hybrid structure.

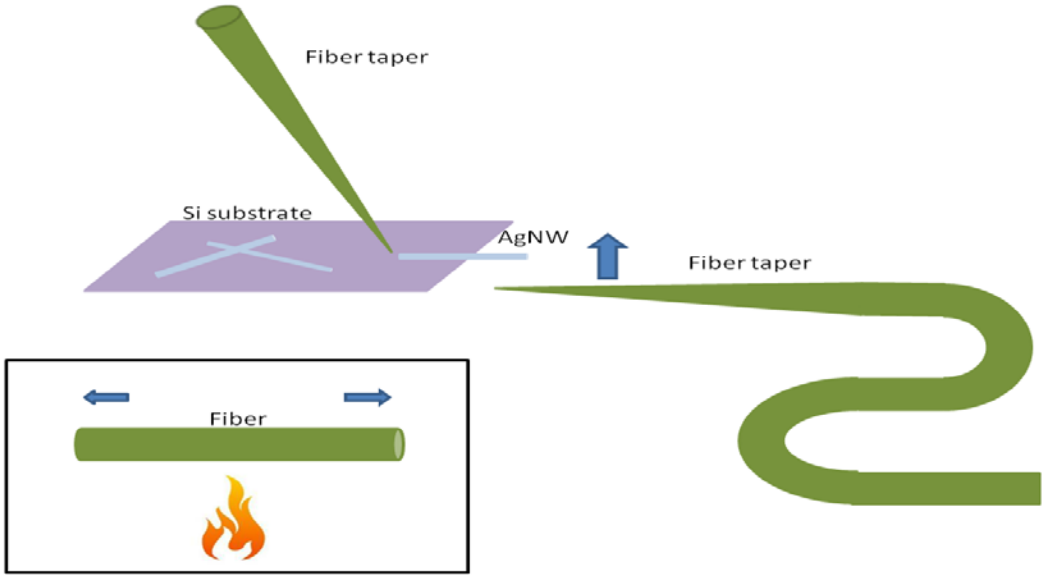

Figure S1. A schematic diagram of the fabrication procedure for the hybrid fiber taper-AgNW waveguide. The insert show a schematic diagram of the fabrication of the fiber taper.

Ⅱ. NUMERICAL SIMULATIONS

We used COMSOL Multiphysics v4.2 to simulate the processes of photon propagation and coupling in a dielectric and a silver nanowire. We first solved for the eigenmodes in uniform waveguides by mode analysis in the two-dimensional radio-frequency module. The stationary electromagnetic-field for the coupling between the fiber taper and the AgNW was then calculated in the three-dimensional frequency domain module with input light at the end of the fiber taper. Scattering boundary conditions were applied in both models.

Figure S2 shows the eigenmodes in a fiber taper and a AgNW with the same radius of $160nm$. The fiber taper can support several kinds of spatial modes and the dominant mode among them for $\lambda = 808nm$ is HE_{11}, which includes two degenerate orthogonal modes. The corresponding electric field distributions are displayed in Fig.S2(a) (labeled M_{0a}) and Fig.S2(b) (labeled M_{0b}).[1] Both have an effective mode index of 1.0292. In addition, the two lowest order SPP modes of a suspended AgNW, as mentioned in the main text are also given in Fig.S2,[2] where the cylindrically symmetric TM_{01} mode with an effective mode index of $n_{\text{i}} = 1.1020 + 0.0048i$ is

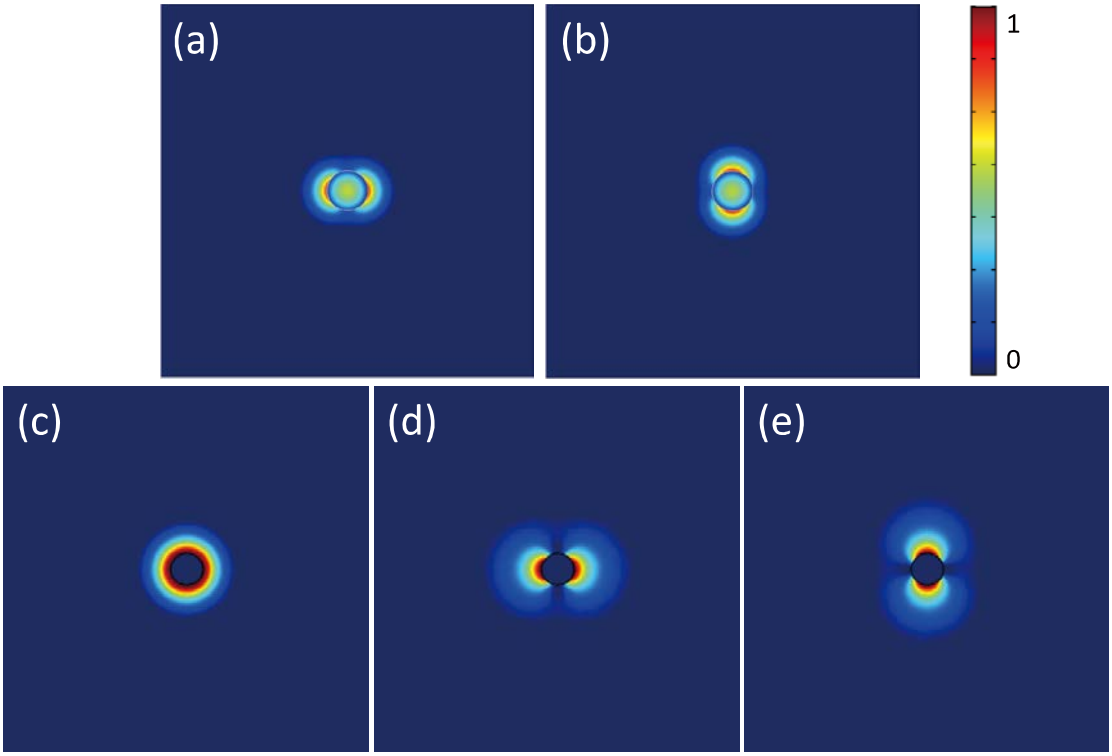

Figure S2. Eigenmodes of the fiber taper and the silver nanowire. (a), (b) HE_{11} mode of the fiber taper (with a radius of 160nm), which supports two orthogonal polarizations and has a degenerate effective mode index of 1.0292. (c) Fundamental TM_{01} mode on the surface of the silver nanowire, which has an effective mode index of $n = 1.1020 + 0.0048i$. (d), (e) Higher-order HE_{11} mode of the free-standing silver nanowire, which similarly supports two orthogonal polarizations and has a degenerate effective mode index of $n = 1.0150 + 0.0017i$.

labeled as H_0 (shown in Fig.S2(c)), and the higher-order SPP mode HE_{11} similarly contains two degenerate orthogonal modes, as shown in Fig.S2(d) (labeled H_{1a}) and Fig.S2(e) (labeled H_{1b}). The common effective mode index of the H_{1a} and H_{1b} modes is calculated to be $n_2 = 1.0150 + 0.0017i$.

Figure S3 shows the real part of the calculated effective mode index of the M_{0b} optical mode as a function of the fiber radius and the electric field distribution of M_{0b} in a bare fiber taper. Thus, for the fiber taper, the effective mode index of M_{0b} varies throughout the coupling process. The effective mode indices of the H_0 and H_{1b} SPP modes are also shown as black and red dotted lines, respectively. Considering the

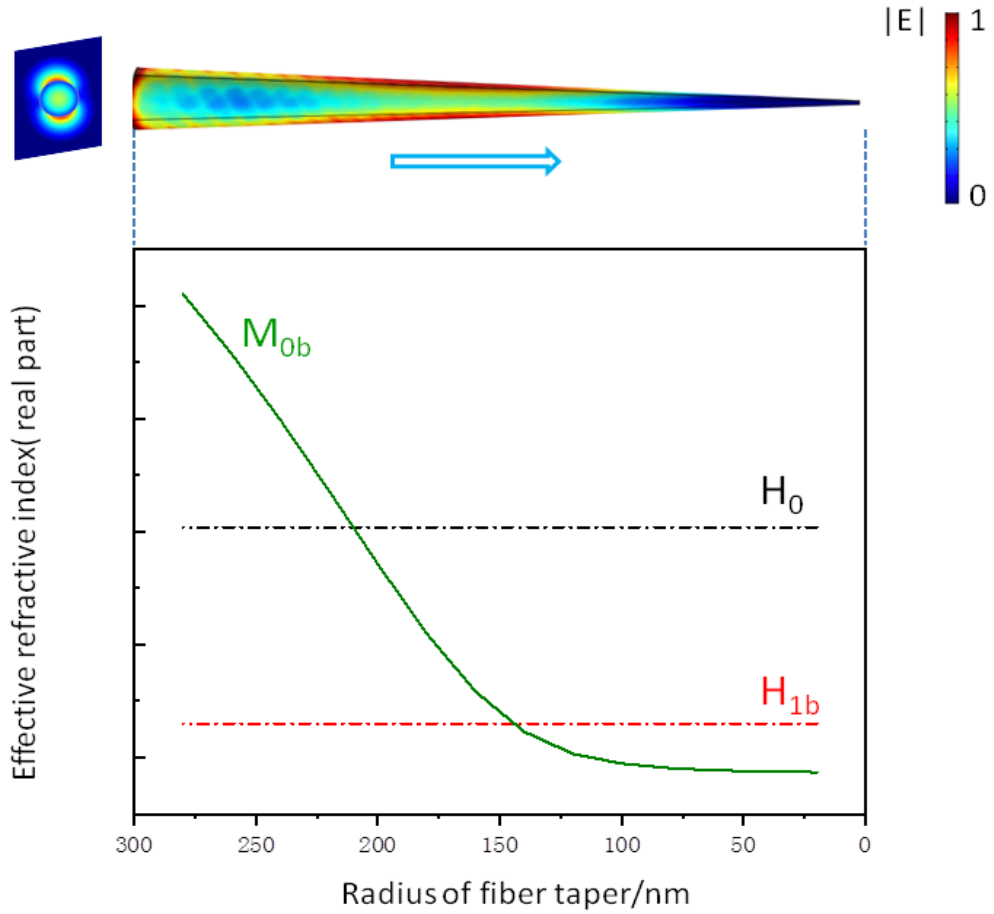

Figure S3. Calculated effective mode indices of the M_{0b} mode (green) with different fiber taper radii and the H_0 SPP mode (black dotted line) and H_{1b} SPP mode (red dotted line) of an AgNW (of 160 nm in radius).

structure of the hybrid fiber taper-AgNW waveguide, the H_{1a} mode in the silver nanowire has the best field overlap with the M_{0a} mode in the fiber taper and thus can be efficiently coupled to the fiber taper, whereas both the H_{1b} and H_0 modes in the silver nanowire have good field overlap with the M_{0b} mode in the fiber taper and thus can both be effectively excited. These findings have been confirmed by our numerical simulations using the three-dimensional frequency-domain module, as shown in the main text. Thus, according to coupled-mode theory, when the M_{0b} mode is input into the fiber taper and propagates along the fiber taper, the energy of the M_{0b} mode should preferentially flow into the H_0 mode first and then into the H_{1b} SPP mode.

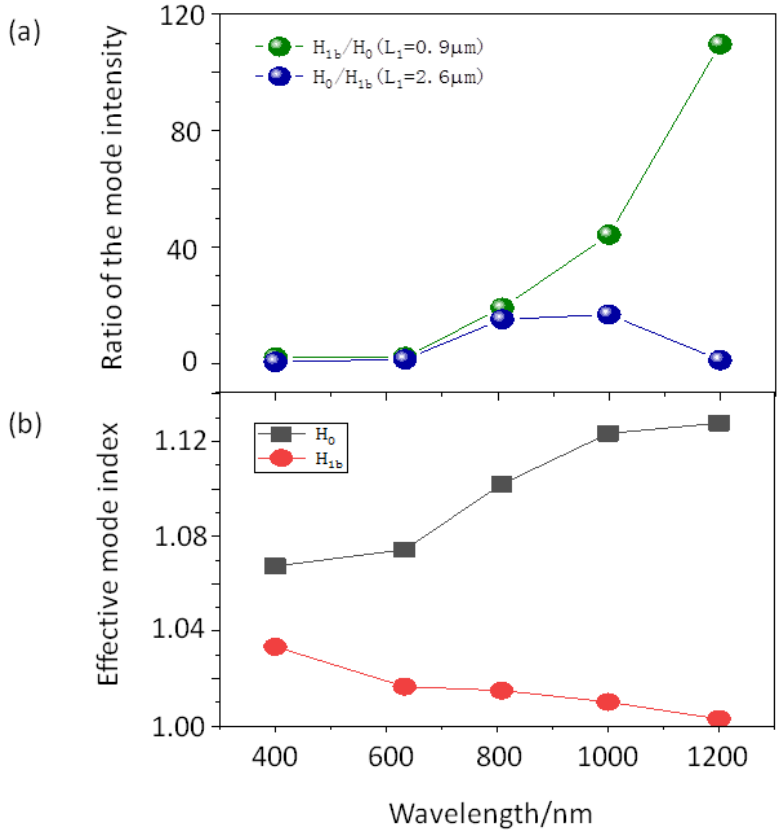

Figure S4. (a) The green data represent the calculated ratio of the H_{1b} mode to the H_0 mode versus the wavelength when the coupling length is $0.9\mu m$, and the blue data represent the calculated ratio of the H_0 mode to the H_{1b} mode versus the wavelength when the coupling length is $2.6\mu m$. (b) Real parts of the effective mode indices for the H_0 and H_{1b} modes versus the wavelength.

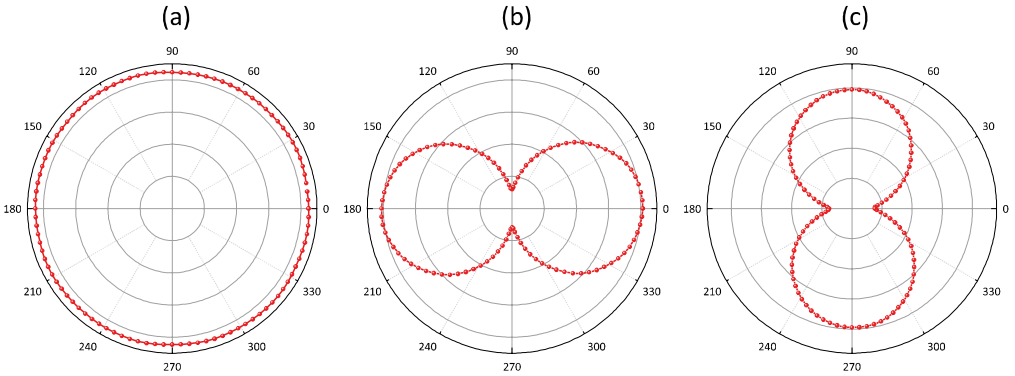

Figure S5. The far-field simulation for the SPP modes of Ag NW (a) H_0, (b) H_{1a} and (c) H_{1b}.

We also discuss how the incident light wavelength influences the excited SPP modes. Because the H_0 and H_{1b} SPP modes have little field overlap with the M_{0a} optical mode, H-polarized incident light will always optimally excite the H_{1a} mode. Here, we mainly consider the situation with V-polarized incident light, and the simulated results are shown in Figure S4(a). When the coupling length is $0.9\ \mu m$, the weight of the H_{1b} mode remains higher than that of the H_0 mode and increases with increasing wavelength. This is because the difference between the effective mode indices of the H_0 and H_{1b} modes is larger for longer wavelengths (see Figure S4(b)), and it becomes harder to excite H_0 with a fiber taper radius of less than 115 nm (the radius of the fiber taper at $0.9\ \mu m$ away from the tip). However, when the wavelength is very short, the difference between the effective mode indices of these two modes is small, whereas when the coupling length is quite long, $2.6\ \mu m$ for instance, both modes can be launched within the coupling region. In this case, adjusting the wavelength does change the dominant excited mode, but the dependence is not a sensitive one.

Figure S5 shows the simulated far-field radiation patterns for H_0, H_{1a} and H_{1b}. Here, the calculation plane is perpendicular to the AgNW, and 0° represents the horizontal direction. A positive correlation between the intensity detected from the far field and the near-field spatial electric field distribution is found. The far-field radiation pattern depends on the SPP modes, and this makes it possible to investigate the SPP modes using far-field methods.

Ⅲ. MEASUREMENT METHOD

The propagation modes in a waveguide that is uniform along the z-axis can be expressed as $\psi(x,y)e^{-ink_0 z}$, where $k_0 = 2\pi / \lambda$ and n is the effective refractive index. The cross section of the silica nanofiber is assumed to be circular, with good geometric symmetry; thus, the transverse electric (H_{1a}) and transverse magnetic (H_{1b}) modes are degenerate. The oscillation direction of the electric field is not restricted to the dielectric fiber taper; thus, the solution to Maxwell's equations shows no change in polarization. When a state $\alpha\left|M_{0a}\right\rangle + \beta\left|M_{0b}\right\rangle$ is input into a nanofiber, the output

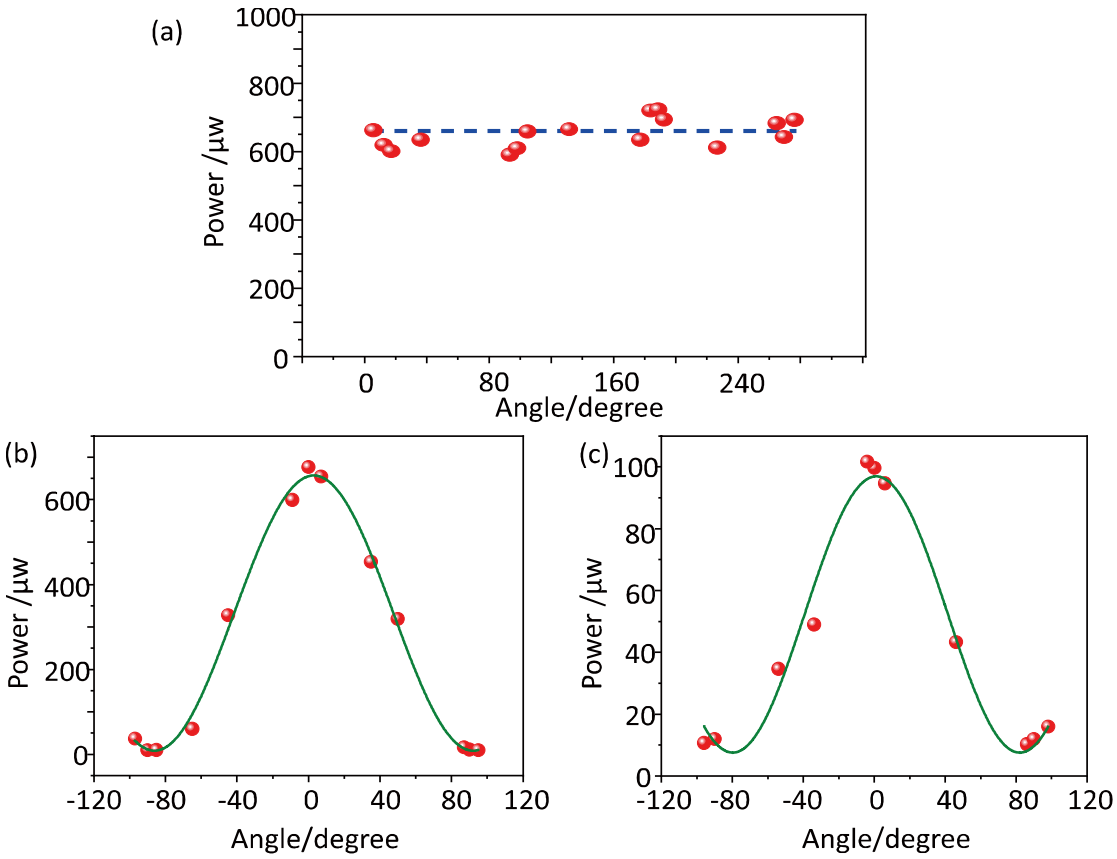

Figure S6. (a) Transmission properties of the fiber taper for different linearly polarized states. We measured the output power while varying the polarization of the input light. Here, 0° denotes the V-polarized state. (b) and (c) show the polarization properties of the fiber taper and the silver nanowire, respectively. The points represent the experimentally measured data, and the green lines represent the curves obtained by fitting the data to a sinusoidal function. With V-polarized input photons, we measured the output power while varying the orientation of the polarizer in front of the power meter. Here, 0° corresponds to V polarization.

state at the end of the nanofiber is expected to be $e^{-inkz}(\alpha|M_{0a}\rangle+\beta|M_{0b}\rangle)$, revealing that the photon polarization will be retained as the photons travel through this symmetric waveguide.[3] We measured the transmission properties of the fiber taper for different linearly polarized states. The resulting curve, which shows only slight fluctuations around $660\mu w$, as seen in Figure S6(a), indicates that the transmission efficiency is insensitive to the polarization of the incident light. Then, we input V-polarized incident radiation and measured the polarization of the output light from

the fiber taper. The fitted curve in Figure 6(b) shows a good extinction ratio of $76.4:1$, proving that the polarization is maintained in the fiber taper.

When second-order SPP modes (H_{1a} and H_{1b}) are excited in the silver nanowire, linear polarizations can be maintained during the energy transfer from the optical modes in the fiber taper to the SPP modes in the silver nanowire. This was demonstrated experimentally, as shown in Figure S6(c), which presents the polarization behavior of the fiber taper-AgNW structure. We measured the output power while rotating the polarizer in front of the power meter; here, 0° on the horizontal axis corresponds to V polarization. The sample used to generate Figure S6(c) was the same as that used to generate Figure 4(a)-4(b) in the main text (sample a). The experimental extinction ratio for V-polarized incident light was measured to be $P_{max} / P_{min} = 12.86$, where P_{max} and P_{min} are the highest and lowest levels of transmission power, respectively, that were measured when rotating the polarizer following the AgNW. This value was depressed by stray light in the environment and could be further improved by using a single-mode fiber for collection. In addition, the shape of the end face of the AgNW and the fundamental mode excited in the AgNW also influenced the measured ratio. These results demonstrate that this kind of hybrid structure can serve as a polarization-maintaining SPP waveguide.

References:

1. Saleh, B. E. A., Teich, M. C. Fundamentals of Photonics, 2nd ed., Wiley: Chichester, United Kingdom, (2007).
2. Barthes, J., Bouhelier, A., Dereux, A., des Francs, G. C., “Coupling of a dipolar emitter into one-dimensional surface plasmon,” Sci. Rep. **3**, 2734 (2013).
3. M. Li, C.-L. Zou, X.-F. Ren, X. Xiong, Y.-J. Cai, G.-P. Guo, L.-M. Tong, and G.-C. Guo, " Transmission of photonic quantum polarization entanglement in a nanoscale hybrid plasmonic waveguide." Nano Lett. **15**, 2380 (2015).